Voltage control of magnetocrystalline anisotropy in ferromagnetic-semiconductor-piezoelectric hybrid structures

A. W. Rushforth,[1] E. De Ranieri,[2] J. Zemen,[3] J. Wunderlich,[2,3] K. W. Edmonds,[1] C. S. King,[1] E. Ahmad,[1] R. P. Campion,[1] C. T. Foxon,[1] B. L. Gallagher,[1] K. Výborný,[3] J. Kučera,[3] and T. Jungwirth[3,1]

[1]*School of Physics and Astronomy, University of Nottingham, Nottingham NG7 2RD, United Kingdom*

[2]*Hitachi Cambridge Laboratory, Cambridge CB3 0HE, United Kingdom*

[3]*Institute of Physics, ASCR v.v.i., Cukrovarnická 10, 162 53 Praha 6, Czech Republic*

(Received 18 January 2008; revised manuscript received 3 June 2008; published 20 August 2008)

We demonstrate voltage control of the magnetic anisotropy of a (Ga,Mn)As device bonded to a piezoelectric transducer. The application of a uniaxial strain leads to a large reorientation of the magnetic easy axis, which is detected by anisotropic magnetoresistance measurements. Calculations based on the mean-field kinetic-exchange model of (Ga,Mn)As provide a microscopic understanding of the measured effect. The reported smooth voltage control of the uniaxial in-plane anisotropy, electrically induced magnetization switching, and detection of unconventional crystalline components of the anisotropic magnetoresistance illustrate the generic utility of our multiferroic system in providing device functionalities and in the research of micromagnetic and magnetotransport phenomena in diluted magnetic semiconductors.

DOI: 10.1103/PhysRevB.78.085314 PACS number(s): 75.50.Pp, 75.47.−m, 75.70.Ak

The control of magnetism by electrical means is an important prerequisite for the successful implementation of spintronics in information processing technologies, and for advancements in sensor and transducer applications. Multiferroic compounds[1,2] or layered structures[3,4] combining piezoelectric/ferroelectric and magnetostrictive/ferromagnetic properties are a promising area of research in this direction. However, due largely to the complex electronic structure and multidomain switching processes that gave rise to complicated hysteresis loops, a microscopic theoretical description of the behavior of these systems is lacking.

The diluted magnetic semiconductor (Ga,Mn)As has many favorable characteristics that can be utilized in a hybrid ferromagnetic/piezoelectric structure. Spin-polarized holes that mediate ferromagnetic coupling between Mn local moments produce large magnetic stiffness, resulting in a mean-field-like magnetization and macroscopic single-domain characteristics.[5,6] At the same time, magnetocrystalline anisotropies derived from spin-orbit coupling effects in the hole valence bands are large and sensitive to strains as small as 10^{-4}.[7,8] The relatively simple band structure allows for a microscopic description of the magnetic[5,9,10] and magnetotransport[11] properties of this system. Finally, the incorporation of semiconductor material in such devices paves the way to the ultimate multifunctional systems, integrating conventional semiconductors with multiferroics.

So far the strain effects in (Ga,Mn)As have been controlled by lattice-parameter engineering during growth[9,10] or through postgrowth lithography.[7,8,12] Here we demonstrate the voltage control, via strain, of the in-plane uniaxial magnetic anisotropy in a (Ga,Mn)As device bonded to a piezotransducer. We follow a technique used previously to produce sizeable strains in nonmagnetic GaAs structures.[13] Microscopic calculations discussed in the second part of the paper describe these effects on an unprecedented level of accuracy compared to rare-earth or metal ferromagnetic/piezoelectric devices.[3,4] We conclude by discussing the realization of electrically induced magnetization switching and of the detection of unconventional crystalline components of the anisotropic magnetoresistance (AMR).

The 25-nm-thick $Ga_{0.94}Mn_{0.06}As$ epilayer was grown by low-temperature molecular-beam epitaxy on GaAs substrate and buffer layers.[14] The material is under compressive in-plane strain of $\sim 3\times 10^{-3}$ (Ref. 15) due to the lattice mismatch with the GaAs. From superconducting quantum interference device (SQUID) magnetometry on the material, the magnetic easy axis is in plane in a direction determined by competition between biaxial [100]/[010] and uniaxial $[1\bar{1}0]$ anisotropies. At 50 K the cubic and uniaxial anisotropy constants determined from hard axis magnetization curves are $K_c = 85\ \mathrm{Jm^{-3}}$ and $K_u = 261\ \mathrm{Jm^{-3}} \pm 20\%$.

A (Ga,Mn)As Hall bar, fabricated by optical lithography and orientated along the $[1\bar{1}0]$ direction, was bonded to the lead zirconate titanate (PZT) piezotransducer using a two-component epoxy after thinning the substrate to $150\pm 10\ \mu$m by chemical etching. The stressor was slightly misaligned so that a positive/negative voltage produces a uniaxial tensile/compressive strain at $\approx -10°$ to the $[1\bar{1}0]$ direction.

The induced strain was measured by strain gauges, aligned along the $[1\bar{1}0]$ and [110] directions, and mounted on a second piece of 150 ± 10-μm-thick wafer bonded to the piezostressor. Differential thermal contraction of GaAs and PZT on cooling to 50 K produces a measured in-plane, biaxial tensile strain at zero bias of 10^{-3}, and a uniaxial strain estimated to be of the order of $\sim 10^{-4}$,[16] which could not be accurately measured. At 50 K, the magnitude of the additional uniaxial strain for a piezovoltage of ± 150 V is approximately 2×10^{-4}.

The orientation of the in-plane magnetization of the (Ga,Mn)As Hall bar was determined from the longitudinal and transverse AMR. To a good approximation ($\approx 10\%$), these are given by $\Delta\rho_{xx}/\rho_{av} = C\cos 2\phi$ and $\rho_{xy}/\rho_{av} = C\sin 2\phi$, where ϕ is the angle between the magnetization direction and the Hall bar direction.[11] Figure 1 shows magnetoresistance measurements at 50 K for external magnetic-

 ©2008 The American Physical Society

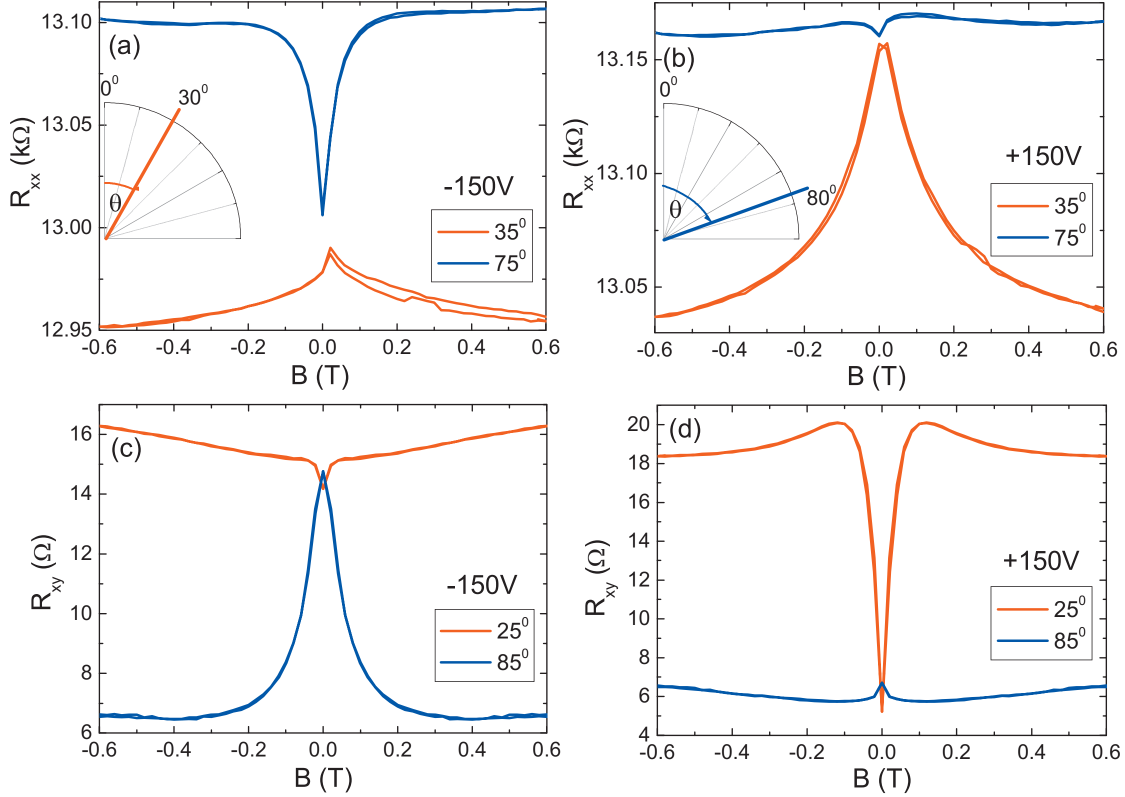

FIG. 1. (Color) [(a) and (b)] The longitudinal resistances R_{xx} and [(c) and (d)] the transverse resistances R_{xy} as a function of magnetic field at angle θ. The curves with θ close to an easy axis (30° at −150 V and 80° at +150 V) are relatively flat as a function of field, indicating small rotation of the angle of the magnetization. T=50 K.

field sweeps at constant field angle θ measured from the Hall bar direction. The strongly θ-dependent low-field magnetoresistance, which saturates at higher field, is due to AMR, i.e., to magnetization rotations. We subtracted an isotropic, θ-independent magnetoresistance contribution from the measured longitudinal resistances. When the external field is close to the magnetic easy axis, the measured resistances at saturation and remanence should be almost the same, and a significant magnetoresistance due to rotation of the magnetization can only be present at very low applied fields. For external fields away from the easy axis, large magnetoresistances corresponding to large rotations of the magnetization orientation are present. This enables us to determine the easy axis directions within ±5°.

The effect of the piezostressor is clearly apparent in Fig. 1. At 50 K, SQUID measurements show that the magnetic easy axis is oriented along the $[1\bar{1}0]$ direction for the as-grown (Ga,Mn)As wafer, consistent with $|K_c|<|K_u|$. The easy axis for the Hall bar bonded to the stressor rotates to an angle ϕ=65° upon cooling to 50 K due to a uniaxial strain induced by anisotropic thermal contraction of the piezostressor.[16] Application of a bias of +150 V to the stressor causes the easy axis to rotate further to ϕ=80° while for −150 V, it rotates in the opposite sense to ϕ=30°. This directly demonstrates electric-field control of the magnetic anisotropy in our (Ga,Mn)As/PZT hybrid system.

The magnetic anisotropy for our system can be described phenomenologically by an energy functional $E(\hat{M})=-K_c/4\sin^2 2\phi+K_u\sin^2\phi+K_u'\sin^2(\phi+\phi_0)$, where the last term with $\phi_0\approx 10°$ is due to the misaligned stressor. The observed behavior is then consistent with the (Ga,Mn)As being in tensile strain along the axis of the stressor on cool down and applied positive (negative) voltage, increasing (decreasing) this strain. Note that the misalignment allows smooth rotation of a single easy axis in the experimentally accessible voltage range.

We now calculate the expected magnetic anisotropy characteristics of the studied (Ga,Mn)As/PZT system. The (Ga,Mn)As electronic structure is obtained by combining the Luttinger Hamiltonian with fixed, GaAs-host band parameters[5,9,10] with the kinetic-exchange model of the coupling to the local Mn_{Ga} d^5 moments, using again a fixed value of the exchange parameter J_{pd}=0.55 meV nm^3.[5,9,10] Unlike the more *ab initio* local-density-approximation approaches, which tend to underestimate the band gap and overestimate the exchange coupling strength, this semiconductor approach is well suited to the description of spin-orbit coupling phenomena near the top of the valence band, which determine the magnetic anisotropies,[5] and also provides a straightforward means of incorporating lattice strains.[7,9,10]

We use the microscopic model to find the dependence of the total-energy density of valence-band holes on the magnetization in-plane angle at a given Mn concentration, hole density, temperature, and in-plane uniaxial strain. This function is then fitted to the phenomenological formula for $E(\hat{M})$, and magnetocrystalline anisotropy constants K_c, K_u, and K_u'

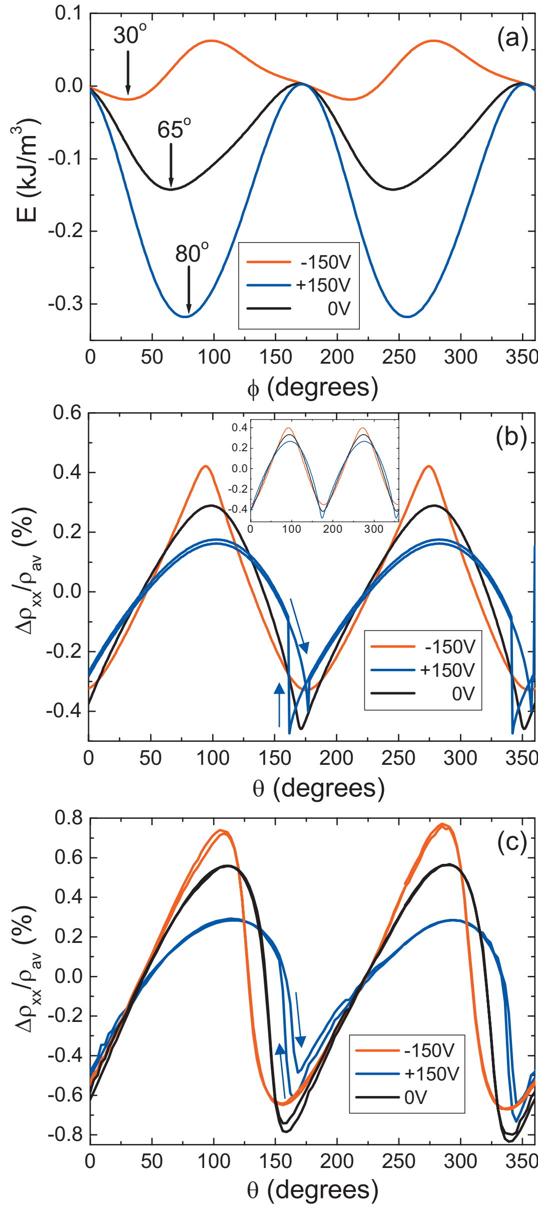

FIG. 2. (Color) (a) The microscopic $E(\hat{M})$ curves for the three piezovoltages. ϕ is the angle of the magnetization with respect to the Hall bar. (b) The longitudinal AMR from theory calculations with a nonsaturating magnetic field of 20 mT rotated clockwise and anticlockwise in the plane of the film. Arrows show the direction of rotation in the hysteretic region. The inset shows the same for a field of 40mT. (c) The experimental AMR curves with a field of 40 mT rotated clockwise and anticlockwise in the plane of the film. ρ_{av} is the ρ_{xx} averaged over 360° in the low-field regime. θ is the angle of the magnetic field with respect to the Hall bar. T=50 K.

are extracted including their dependence on material parameters.

Due to the presence of unintentional compensating defects, the concentrations of ferromagnetically ordered Mn local moments ($N_{\rm Mn}$) and holes (p) cannot be accurately controlled during growth or determined postgrowth.[17] The magnetocrystalline anisotropy constants are known to be sensitive to the local-moment density and the hole compensation ratio $p/N_{\rm Mn}$. To guarantee that the comparison be-

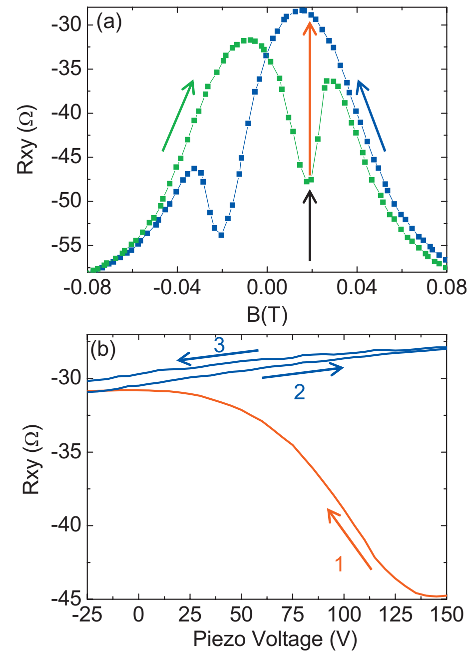

FIG. 3. (Color) (a) Low-field magnetic hysteresis curve at +150 V. The field is swept from saturating negative field at 165° to the position shown by the black arrow. Then (b) the piezovoltage is swept, inducing a rotation of the angle of the magnetization indicated by the red arrows. Numbered arrows represent the order and direction of the voltage sweeps. T=30 K.

tween theory and experiment does not suffer from an accidental choice of p and $N_{\rm Mn}$ in the calculations, we consider simultaneously $\rm Mn_{Ga}$ dopings within an interval x=3–5%, which safely contains the expected value of x in the experimental sample ($N_{\rm Mn}=4x/a_{lc}^3$, where a_{lc} is the lattice parameter). First, we focus on the bare sample at 50 K. The cubic term K_c is calculated without adjustable band parameters (as emphasized above) for each $N_{\rm Mn}$ from the relevant interval and for a fixed compensation ratio $p/N_{\rm Mn}$. The result is in good agreement with the measured 50 K K_c for $p/N_{\rm Mn}$=0.6 at x=3%, decreasing smoothly to $p/N_{\rm Mn}$=0.4 at x=5%. These values are in good agreement with the estimated compensation ratio in our as-grown material.[17]

The origin of the uniaxial anisotropy term in bare

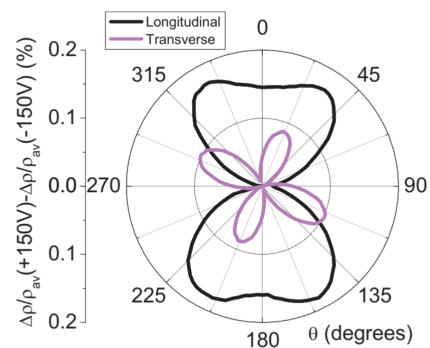

FIG. 4. (Color) The change in the longitudinal $\Delta\rho_{xx}/\rho_{av}$ and the transverse $\Delta\rho_{xy}/\rho_{av}$ components of the AMR for piezovoltages of ±150 V. For clarity, the y axis is offset for each curve so that the minimum is at zero.

(Ga,Mn)As wafers is not known but it can be modeled[7,18] by introducing a shear strain $e_{\rm int}$ along the $[1\bar{1}0]$ axis. For $p/N_{\rm Mn}=0.6-0.4$, we obtain the experimental value of K_u for compressive shear strain $e_{\rm int}=3-2\times10^{-4}$ within the considered range of x's.

Having fixed $e_{\rm int}$, which is the only adjustable parameter in our model, we study the sample attached to the piezostressor. The additional in-plane strain is described by a term in the Hamiltonian analogous to the "intrinsic" uniaxial strain but rotated by 10° due to the misaligned stressor. The calculations reproduce the measured 0 V easy axis for a tensile strain of $e_{\rm str}=6-4\times10^{-4}$ along the stressor axis and the experimental easy axes for ±150 V are obtained by increasing/decreasing the $e_{\rm str}$ strain by $3-2\times10^{-4}$. These *changes* in strain agree with the measured values for ±150 V and the 0 V strain due to differential contraction is of the expected order. The resulting microscopic $E(\hat{M})$ curves for the three voltages are shown in Fig. 2(a).

The magnetoresistance calculated microscopically from the same band-structure model combined with Boltzmann transport theory[11] gives AMR at saturation of the same sign and comparable magnitude to the experiment if we assume the above compensation ratios. This allows us to microscopically simulate AMR measurements assuming, as in previous micromagnetics studies of (Ga,Mn)As,[6] the single domain behavior. In Fig. 2(b) we show the results of simulations and in Fig. 2(c), we show experimental data for the situation where a magnetic field of magnitude smaller than the saturation field is rotated in the plane of the (Ga,Mn)As epilayer. Both theory and experiment show that these AMR traces are no longer sinusoidal since the magnetization does not track the applied rotating field. Ranges of magnetic-field angles θ for which resistance is more slowly varying correspond to angles close to the easy axis. Rotation around the hard axis is more abrupt and in this region the AMR can develop hysteretic features whose widths increase with decreasing magnitude of the rotating field. [To highlight the possibility for the hysteretic behavior in the single-domain model, we show in Fig. 2(b) calculations for 20 mT field with large hysteresis; at 40 mT used in experiment, the hysteresis is unresolved in the theory data.] At +150 V the hard axis is close to the Hall bar axis, resulting in sharper minima than maxima in the corresponding experimental and theoretical AMR traces, while the trend is clearly opposite for the −150 V bias data, consistent with the easy axis directions obtained from the field sweep measurements.

We now proceed with the demonstration of an electrically induced magnetization switching. The bias-dependent hysteresis loops that allow for such a reversal process are shown in Fig. 3(a). With the piezovoltage at +150 V, the initial magnetization state is prepared by sweeping the external magnetic field from negative saturating field at 165° to the position shown by the black arrow. This causes the magnetization to rotate from 165° to 260°, at $B=0$ T (i.e., along the easy axis at +150 V), then to 275° for the small positive field of approximately 18 mT (marked by the black arrow). Then, with the external magnetic field held constant, the piezovoltage is swept [Fig. 3(b)] and the magnetization rotates from 275° to 25° (i.e., close to the easy axis for −150 V) resulting in a change of R_{xy}, as shown by the red arrows. (The few Ohms discrepancy in the initial value of R_{xy} arises due to the 2 mT resolution of our magnet.) This sequence switches the magnetization from the 4th to the 1st quadrant, where it remains for subsequent voltage sweeps. The magnetization can be switched back again by reversing the sequence with the magnetic field set to the opposite polarity.

Finally, we report on the detection of an unconventional crystalline component of the AMR allowed by the piezovoltage control. The AMR in (Ga,Mn)As is known to consist of a noncrystalline component, reflecting the symmetry breaking imposed by a preferred current direction, and crystalline terms reflecting the underlying crystal symmetry. The crystalline terms typically represent 10% of the total AMR in 25 nm (Ga,Mn)As layers.[11] Figure 4 shows the change in the longitudinal $\Delta\rho_{xx}/\rho_{av}$ and transverse $\Delta\rho_{xy}/\rho_{av}$ components of the AMR for piezovoltages of ±150 V. $\Delta\rho_{xx}=\rho_{xx}-\rho_{av}$, and ρ_{av} is the average of ρ_{xx} over 360° in the plane. The distortion of the lattice by the piezotransducer leads to modification of the crystalline components of the AMR, shown in the figure by subtracting the curves at piezovoltages of ±150 V. This modification represents $\approx10\%$ of the total AMR and is comparable to the absolute magnitude of the crystalline terms. The appearance of a fourth-order term in the transverse AMR is expected under a uniaxial distortion[19] but this higher order term was unresolved in the bare (Ga,Mn)As layers.[11]

To conclude, we have demonstrated the voltage control of the magnetic anisotropy and AMR, and nonvolatile switching of the magnetization direction in (Ga,Mn)As induced by strain applied with a piezoelectric transducer. Microscopic theory calculations capture the physics involved. Recently, we have become aware of two groups who have presented results on similar PZT/(Ga,Mn)As hybrid structures.[20]

We are grateful to J. Chauhan and D. Taylor for sample fabrication. We acknowledge support from EU Grant No. IST-015728, from UK Grant No. GR/S81407/01, from CR Grants No. 202/05/0575, No. 202/04/1519, No. FON/06/E002, No. AV0Z1010052, No. KJB100100802, No. LC510, and No. KAN400100652, and from U.S. Grant NRI SWAN.

[1] R. Ramesh and N. A. Spaldin, Nat. Mater. **6**, 21 (2007).

[2] J. Hemberger, P. Lunkenheimer, R. Fichtl, H. A. Krug von Nidda, V. Tsurkan, and A. Loidl, Nature (London) **434**, 364 (2005).

[3] T. Wu, M. A. Zurbuchen, S. Saha, R. V. Wang, S. K. Streiffer, and J. F. Mitchell, Phys. Rev. B **73**, 134416 (2006); J. G. Wan, J. M. Lui, G. H. Wang, and C. W. Nan, Appl. Phys. Lett. **88**, 182502 (2006); K. Dorr and C. Thiele, Phys. Status Solidi B

243, 21 (2006).

[4] Sang-Koog Kim, Jeong-Won Lee, Sung-Chul Shin, Han Wook Song, Chang Ho Lee, and Kwangsoo No, J. Magn. Magn. Mater. **267**, 127 (2003); Jeong-Won Lee, Sung-Chul Shin, and Sang-Koog Kim, Appl. Phys. Lett. **82**, 2458 (2003); Bernhard Botters, Fabian Giesen, Jan Podbielski, Peter Bach, Georg Schmidt, Laurens W. Molenkamp, and Dirk Grundler, *ibid.* **89**, 242505 (2006); H. Boukari, C. Cavaco, W. Eyckmans, L. Lagae, and J. Borghs, J. Appl. Phys. **101**, 054903 (2007).

[5] T. Jungwirth, Jairo Sinova, J. Mašek, J. Kučera, and A. H. MacDonald, Rev. Mod. Phys. **78**, 809 (2006).

[6] K. Y. Wang, M. Sawicki, K. W. Edmonds, R. P. Campion, S. Maat, C. T. Foxon, B. L. Gallagher, and T. Dietl, Phys. Rev. Lett. **95**, 217204 (2005).

[7] J. Wunderlich, A. C. Irvine, J. Zemen, V. Holý, A. W. Rushforth, E. De Ranieri, U. Rana, K. Výborný, Jairo Sinova, C. T. Foxon, R. P. Campion, D. A. Williams, B. L. Gallagher, and T. Jungwirth, Phys. Rev. B **76**, 054424 (2007).

[8] J. Wenisch, C. Gould, L. Ebel, J. Storz, K. Pappert, M. J. Schmidt, C. Kumpf, G. Schmidt, K. Brunner, and L. W. Molenkamp, Phys. Rev. Lett. **99**, 077201 (2007).

[9] T. Dietl, H. Ohno, and F. Matsukura, Phys. Rev. B **63**, 195205 (2001).

[10] M. Abolfath, T. Jungwirth, J. Brum, and A. H. MacDonald, Phys. Rev. B **63**, 054418 (2001).

[11] A. W. Rushforth, K. Výborný, C. S. King, K. W. Edmonds, R. P. Campion, C. T. Foxon, J. Wunderlich, A. C. Irvine, P. Vašek, V. Novák, K. Olejník, Jairo Sinova, T. Jungwirth, and B. L. Gallagher, Phys. Rev. Lett. **99**, 147207 (2007).

[12] S. Hümpfner, K. Pappert, J. Wenisch, K. Brunner, C. Gould, G. Schmidt, L. W. Molenkamp, M. Sawicki, and T. Dietl, Appl. Phys. Lett. **90**, 102102 (2007).

[13] M. Shayegan, K. Karrai, Y. P. Shkolnikov, K. Vakili, E. P. De Poortere, and S. Manus, Appl. Phys. Lett. **83**, 5235 (2003).

[14] R. P. Campion, K. W. Edmonds, L. X. Zhao, K. Y. Wang, C. T. Foxon, B. L. Gallagher, and C. R. Staddon, J. Cryst. Growth **251**, 311 (2003).

[15] L. X. Zhao, C. R. Staddon, K. Y. Wang, K. W. Edmonds, R. P. Campion, B. L. Gallagher, and C. T. Foxon, Appl. Phys. Lett. **86**, 071902 (2005).

[16] B. Habib, J. Shabani, E. P. De Poortere, M. Shayegan, and R. Winkler, Appl. Phys. Lett. **91**, 012107 (2007).

[17] T. Jungwirth, J. Mašek, K. Y. Wang, K. W. Edmonds, M. Sawicki, M. Polini, Jairo Sinova, A. H. MacDonald, R. P. Campion, L. X. Zhao, N. R. S. Farley, T. K. Johal, G. van der Laan, C. T. Foxon, and B. L. Gallagher, Phys. Rev. B **73**, 165205 (2006).

[18] M. Sawicki, K.-Y. Wang, K. W. Edmonds, R. P. Campion, C. R. Staddon, N. R. S. Farley, C. T. Foxon, E. Papis, E. Kamińska, A. Piotrowska, T. Dietl, and B. L. Gallagher, Phys. Rev. B **71**, 121302(R) (2005).

[19] E. De Ranieri, A. W. Rushforth, K. Vyborny, U. Rana, E. Ahmad, R. P. Campion, C. T. Foxon, B. L. Gallagher, A. C. Irvine, J. Wunderlich, and T. Jungwirth, New J. Phys. **10**, 065003 (2008).

[20] M. Overby, A. Chernyshov, L. P. Rokhinson, X. Liu, and J. K. Furdyna, Appl. Phys. Lett. **92**, 192501 (2008); S. T. B. Goennenwein, M. Althammer, C. Bihler, A. Brandlmaier, S. Geprägs, M. Opel, W. Schoch, W. Limmer, R. Gross, and M. S. Brandt, Phys. Status Solidi (RRL) **2**, 96 (2008).